Available online at www.sciencedirect.com
SCIENCE DIRECT
Journal of Catalysis 235 (2005) 341–352
JOURNAL OF CATALYSIS
www.elsevier.com/locate/jcat

Formation of nanosized zirconia-supported 12-tungstophosphoric acid in mesoporous silica SBA-15: A stable and versatile solid acid catalyst for benzylation of phenol

Dhanashri P. Sawant [a], A. Vinu [b], Nalini E. Jacob [a], F. Lefebvre [c], S.B. Halligudi [a,*]

[a] *Inorganic Chemistry & Catalysis Division, National Chemical Laboratory, Pune 411 008, India*
[b] *International Center for Young Scientists, National Institute for Materials Science, 1-1, Namiki, Tsukuba, Ibaraki 305-0044, Japan*
[c] *Laboratoire de Chimie Organométallique de Surface, CNRS-CPE, Villeurbanne cedex, France*

Received 29 April 2005; revised 9 August 2005; accepted 16 August 2005

Abstract

A nanosized zirconia-supported 12-tungstophosphoric acid (TPA) in SBA-15 composite was prepared by wet impregnation of TPA/ZrO_2 nanoparticles inside the mesoporous channels of SBA-15. The resulting composite material was calcined at 1123 K and characterized by elemental analysis, powder X-ray diffraction, nitrogen adsorption isotherms, transmission electron microscopy (TEM), scanning electron microscopy (SEM), solid-state ^{31}P CP-MAS NMR, ^{29}Si MAS NMR, UV–vis diffuse reflectance spectra, FTIR, TPD of ammonia, FTIR pyridine adsorption, and thermogravimetric analysis (TG-DTG). The synthesized TPA/ZrO_2/SBA-15 showed a well-ordered hexagonal mesoporous structure and mesoporous support SBA-15 stabilized ZrO_2-t (tetragonal) phase with crystal size in the range of 3–4 nm. SBA-15 was a better support than MCM-41 and MCM-48 because it retained its mesostructure even after high TPA loading and high calcination temperatures. Mesoporous silica support plays an important role in stabilizing the catalytically active tetragonal phase of zirconia, which gave the most active catalysts. The catalysts were examined for their catalytic activities in the liquid phase benzylation of phenol with benzyl alcohol and the catalyst 15 wt% TPA/22.4 wt% ZrO_2/SBA-15 calcined at 1123 K was found to have high acidity and to be 10 times more active than neat TPA/ZrO_2 under the reaction conditions studied in benzylation of phenol.

Keywords: Nanosized; Tetragonal phase; TPA/ZrO_2; Phenol benzylation reaction

1. Introduction

Many solid acid catalysts have replaced conventional inorganic acids, such as HF and H_2SO_4, for acid-catalyzed transformations, which causes environmental pollution [1]. Among these, zeolites [2–4] dominate the scenario, and some isolated studies have been reported with supported heteropoly acid (HPA) catalysts [5–9]. Zirconia modified with tungstophosphoric acid forms a highly acidic catalytic phase with an excellent catalytic activity in a variety of acid-catalyzed reactions [10,11]. Sulfated and tungstated zirconia are highly acidic catalysts, but their well-known drawbacks restrict their use in acid-catalyzed reactions [12–14]. Hence there is a need to develop new catalysts that are more active and thermally and hydrothermally stable for applications as solid acid catalysts.

Newly developed silica mesoporous molecular sieves have attracted much interest because of their high surface area, large pore volume, and uniform hexagonal arrays, which provide the potential for use as catalysts or as catalyst support [15,16]. Pure HPAs have strong Brönsted acidity and have been widely investigated in numerous acid-catalyzed reactions [17–19]. However, because of low surface area and high solubility in polar solvents, their use in supported forms, especially over high-surface area materials, has attracted much attention [20–24]. In general, HPAs interact strongly with the supports at low loading levels, whereas the bulk properties of HPA prevail at high loading levels [25–27]. The anchorage quality of HPA is related to the

* Corresponding author.
E-mail address: halligudi@cata.ncl.res.in (S.B. Halligudi).

0021-9517/$ – see front matter
doi:10.1016/j.jcat.2005.08.010

Brönsted acidity of the support. If the support is strongly basic (e.g., Al_2O_3, MgO), the interaction with HPA is too strong, and it will undergo a loss in crystallinity of the heteropolyacid with a complete degradation of the storage properties. If the support is strongly acidic (e.g., SiO_2), then the storage remains possible, and the structure of the heteropolyacid exists, although the anchorage is not secured and the submission of a monolith to a dry air flow will lead to the loss of HPA in the stream. In the case of medium acidity (e.g., TiO_2, SnO_2), the structural properties are maintained, and the absorption capacity is high. So, in general, it is possible to conclude that HPA structure could be well preserved on solids with an isoelectric point around 7 [28]. Cerium and zirconium oxides fit this latter case. Mesoporous silica (MS) like SBA-15 [29] has very large surface area, large pore volume, and high thermal and hydrothermal stability, with large and uniform pore size. Therefore, we used SBA-15 as support to prepare nanosized zirconia-supported TPA composite catalysts for their applications in catalysis. A promising technique for the impregnation of nanoparticles into well-defined architecture is their deposition over ordered mesostructures. According to the literature, TiO_2 and ZrO_2 [30] phases and sulfated zirconia [31] have been inserted into SBA-15 by chemical solution decomposition (CSD) and internal hydrolysis for keeping the mesoporous structure intact even after modification. In the present study, we demonstrate that simple impregnation and controlled calcination retain the mesoporous structure of silica supports like SBA-15. Other mesoporous supports, including MCM-41 and MCM-48, were also used for comparison in this study.

Alkylation of phenol with different alcohols is an industrially important in production of various products [32,33]. Benzylation of phenol by benzyl alcohol (BA) to benzyl phenol (BP) is an important reaction, and BPs are useful raw materials for producing antioxidants and plastic, rubber, and petroleum products [34]. The present work deals with the role of mesoporous support and how its properties influences over the catalytic activity of neat TPA/ZrO_2 in an acid-catalyzed benzylation as a test reaction. Our findings demonstrate that TPA/ZrO_2 dispersed uniformly in nanosized channels of SBA-15 and provided strong acidity and catalytic activity compared with neat TPA/ZrO_2 catalyst in a phenol benzylation reaction.

2. Experimental

2.1. Materials

Samples were synthesized with hexadecyltrimethylammonium bromide (Aldrich); tetraethylorthosilicate (Aldrich); a triblock copolymer of ethylene oxide (EO) and propylene oxide (PO), $EO_{20}PO_{70}EO_{20}$ (Pluronic P123) (Aldrich, $M_{avg} = 5800$); zirconium oxychloride $ZrOCl_2 \cdot 8H_2O$ (Merck); and 12-tungstophosphoric acid (TPA) (Merck) used without further purification. Phenol and benzyl alcohol (BA) were procured from Aldrich.

2.2. Catalyst preparation

Pure siliceous SBA-15, MCM-41, and MCM-48 were synthesized according to literature [35–37]. The gel chemical composition for SBA-15 was 4 g polymer: 0.041 mol TEOS: 0.24 mol HCl: 6.67 mol H_2O. The molar ratio of the synthesis gel composition was 10 SiO_2:5.4 $C_nH_{2n+1}(CH_3)_3NBr$: 4.24 Na_2O:1.3 H_2SO_4:480 H_2O for MCM-41 and 1 M TEOS: 0.25 M Na_2O:0.65 M $C_{16}H_{33}(CH_3)_3NBr$:0.62 M H_2O for MCM-48. The as-synthesized mesoporous samples were calcined in air at 540 °C for 8 h.

TPA/ZrO_2/MS composite materials were prepared in two steps. First, pure siliceous SBA-15 was impregnated with an aqueous solution of $ZrOCl_2 \cdot 8H_2O$ with a predetermined ZrO_2: SBA-15 (22.4%) weight ratio, and the same amount of zirconia loading was used over MCM-41, which corresponded to monolayer coverage [38]. The resulting mixture was stirred in a rotary evaporator for 2–3 h followed by evaporation to dryness and dried at 373 K for 12 h and powdered well for further use. Then, a series of catalysts with different TPA loadings were prepared by suspending a known amount of an aqueous solution of TPA (10–12 ml distilled water) per g of dried ZrO_2/SBA-15 support. This mixture was stirred in a rotary evaporator for 2–3 h followed by evaporation to dryness and the samples were dried at 373 K for 12 h, powdered, and calcined at 1123 K in air for 4 h. TPA/ZrO_2 over other mesoporous silica supports, including MCM-41 and MCM-48, were also synthesized following a similar procedure. For studying the effect of zirconia addition, a catalyst sample without ZrO_2 was synthesized by impregnating an aqueous solution of 3.36 wt% TPA over SBA-15 following same procedure described earlier. The effect of adding TPA was studied by synthesizing a catalyst without TPA, which was prepared by impregnating 22.4 wt% zirconia over SBA-15. The solvent was evaporated to dryness, then dried and calcined at 1123 K for 4 h. Neat 15 wt% TPA/ZrO_2 was synthesized by mixing aqueous solutions of TPA with zirconium oxychloride; then the solvent was evaporated, and the resulting material was dried and calcined at 1123 K under air for 4 h.

2.3. Characterization of the catalysts

Zr, W, and P content in the resulting solids were determined by inductively coupled plasma-optical emission spectroscopy (ICP-OES) and EDAX, using a Bruker small-angle X-ray scattering (SAXS) instrument with general area detector diffraction (GADDS) using Cu-K_α radiation at steps of 0.01°. SAXS pattern of the samples was obtained in reflection mode using a Rigaku Dmax 2500 diffractometer and Ni-filtered copper radiation. Low-angle XRD of neat SBA-15 and different TPA-loaded catalysts were scanned in the range $2\theta = 0.5$–10°, and the generator was operated at 40 kV and 150 mA. The wide reflections in the X-ray diffractogram at $2\theta \approx 30$, 50, and 60° characteristic of the ZrO_2-t (tetragonal) phase were detected using X-ray powder diffraction with Cu-K_α radiation ($\lambda = 1.5418$ Å; Rigaku model D/MAXIII VC, Japan). The tetragonal crystallite size of the various samples was estimated from integral line

width using the Scherrer relationship [39]

$$D_{hkl} = 0.9\lambda / B_{hkl} \cos\theta,$$

where B_{hkl} is the effective line width of the X-ray reflection.

The specific surface area, pore volume, and pore size distribution of samples were measured with an Omnisorb 100CX (Coulter, USA) system under liquid N_2 temperature, using N_2 as an adsorbent.

Formation of ZrO_2-t nanoparticles in the nanotubular channels of calcined 15 wt% TPA/22.4 wt% ZrO_2/SBA-15 was detected by TEM (a JEOL Model 1200 EX operated at an accelerating voltage at 120 kV). Samples were prepared by placing droplets of a suspension of the sample in isopropanol on a polymer microgrid supported on a Cu grid for TEM measurements. The morphology of the catalytic material was determined by JEOL-JSM-5200 SEM with a resolution of 5.5 nm.

The state of TPA in the catalyst and retention of mesoporosity of the silica support were elucidated by ^{31}P CP-MAS NMR (Bruker DSX 300-MHz spectrometer) and ^{29}Si MAS NMR (Bruker DRX 500-MHz spectrometer), respectively. ^{31}P CP-MAS NMR was recorded at 121.5 MHz with high-power decoupling with a Bruker 4-mm probehead. The spinning rate was 10 kHz, and the delay between two pulses was varied between 1 and 30 s, to ensure complete relaxation of the ^{31}P nuclei. The chemical shifts are given relative to external 85% H_3PO_4.

DRS spectrum for solid samples were recorded in the range of 200–600 nm using a Shimadzu UV-2101PC spectrophotometer fitted with a diffuse reflectance chamber with inner surface of $BaSO_4$. A Shimadzu FTIR-8201PC unit, in DRS mode and with a measurement range of 600–1200 cm^{-1}, was used to obtain the FTIR spectra of solid samples.

The total amount of acidity present in the catalyst was estimated using temperature-programmed desorption (TPD) of NH_3 on a Micromeritics AutoChem 2910 instrument. It was done by dehydrating 0.1 g of the catalyst sample at 500 °C in dry air for 1 h and then purged with helium for 0.5 h. The temperature was decreased to 125 °C under the flow of helium, and then 0.5 ml NH_3 pulses were supplied to the samples until no more uptake of NH_3 was observed. NH_3 was desorbed in He flow by increasing the temperature to 540 °C with a heating rate of 10 °C min^{-1} measuring NH_3 desorption using a TCD detector.

The nature of acid sites (Brönsted and Lewis) of the catalyst samples with different loading were characterized by in situ Fourier transform infrared (FTIR) spectroscopy with chemisorbed pyridine in drift mode on an FTIR-8300 Shimadzu SSU-8000 instrument with 4 cm^{-1} resolution and averaged over 500 scans. These studies were performed by heating precalcined powder samples in situ from room temperature to 400 °C with a heating rate of 5 °C min^{-1} in a flowing stream (40 ml min^{-1}) of pure N_2. The samples were kept at 400 °C for 3 h and then cooled to 100 °C; then pyridine vapors (20 µl) were introduced under N_2 flow, and the infrared (IR) spectra were recorded at different temperatures up to 400 °C. A resolution of 4 cm^{-1} was attained after averaging over 500 scans for all the IR spectra recorded here.

Thermogravimetric analysis (TG-DTG) measurements were performed on a Setaram TG-DTA 92 apparatus from room temperature to 1000 °C in flowing dry air (ca. 50 ml min^{-1}), using α-Al_2O_3 as a reference. Each experiment used 25–30 mg of the sample, with a heating rate of 10 °C min^{-1}. TGA curves are depicted as first-derivative DTGs of the direct weight loss traces.

2.4. Benzylation of phenol by benzyl alcohol

The benzylation of phenol by BA has been used as a probe reaction for studying catalytic properties. The reaction was carried out in a 50-ml round-bottomed flask under continuous stirring equipped with condenser, a nitrogen inlet for maintaining an inert atmosphere, and an additional port for sample withdrawal. Temperature was maintained by placing this assembly in a thermostatted oil bath. The reaction was carried out at selected reaction conditions, at 363 K with a 6:1 phenol:BA molar ratio and with 5 wt% (total reaction mixture) of catalyst. Clear liquid samples withdrawn periodically were analyzed by gas chromatography (GC) with a capillary column and a flame ionization detector. The conversions were based on the consumed BA in the reaction mixture. The products were confirmed by GC-mass spectroscopy (GC-MS) and GC-IR.

3. Results and discussion

3.1. Characterization of the catalysts

The X-ray powder diffraction patterns of the catalysts with different (%) TPA loadings calcined at 1123 K are shown in Fig. 1a, and those of 15 wt% TPA/22.4 wt% ZrO_2/SBA-15 calcined at different calcination temperatures are shown in Fig. 1b. The small angle X-ray diffraction patterns of TPA/ZrO_2 modified samples were typical of hexagonally ordered mesoporous materials, with one sharp peak indexed as (100) and two smaller peaks indexed as (110) and (200), typical of hexagonal ($p6mm$) of parent SBA-15. Fig. 1a shows that the mesoporous structure that remained intact at up to 50 wt% TPA loading started to lose mesoporosity. In addition, the 15 wt% TPA-loaded sample showed intact mesoporosity even after calcination up to 1273 K. The added TPA stabilized the tetragonal phase of zirconia. Such stabilization of the phase composition desired for specific applications in the presence of other mesoporous oxides prevented the particles from growing larger than the pore sizes. XRD patterns displayed three well-defined peaks characteristic of tetragonal ZrO_2; these can be indexed as (111), (202), and (131). Wide-angle XRD of TPA over 22.4 wt% ZrO_2/SBA-15 up to 15 wt% loading of TPA shows monolayer coverage; above this, it started showing WO_3 (23.12, 23.59, and 24.38°) crystalline peaks due to partial decomposition of TPA, as shown in the inset of Fig. 1a. Similarly, 15 wt% TPA/22.4 wt% ZrO_2/SBA-15 showed monolayer coverage up to 1123 K calcination temperature. However, above 1123 K, it showed decomposition of TPA into WO_3 crystallites (inset of Fig. 1b). As for bulk zirconia, crystallization of the amorphous phase to the metastable tetragonal phase typically occurred at 673–773 K, but after loading

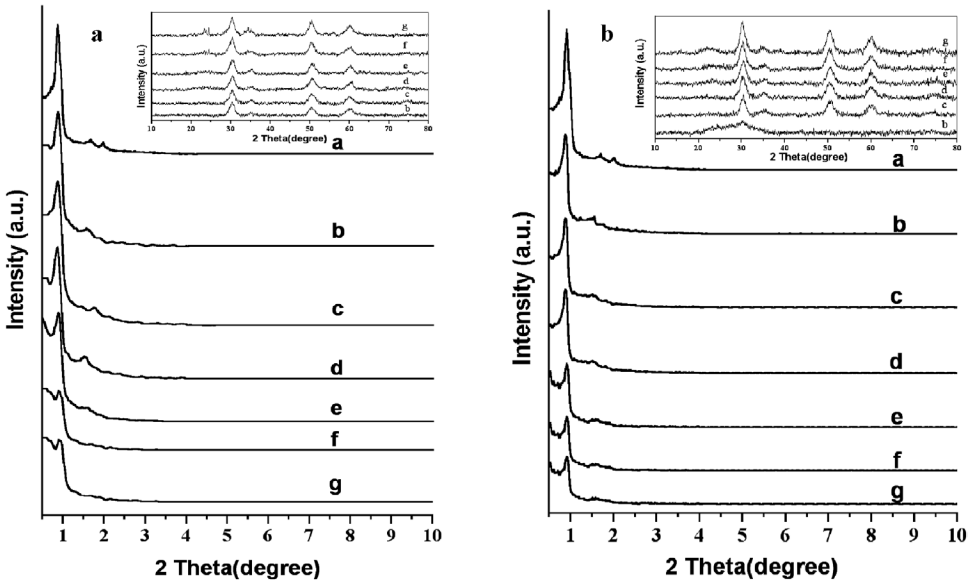

Fig. 1. (a) Low angle XRD: a, SBA-15, TPA/22.4 wt% ZrO_2/SBA-15 with: b, 5; c, 15; d, 30; e, 50; f, 70; and g, 90 wt% TPA loading and calcined at 1123 K, including insight wide-angle XRD, respectively. (b) Low angle XRD: a, SBA-15, 15 wt% TPA/22.4 wt% ZrO_2/SBA-15 calcined at: b, 923; c, 1023; d, 1123; e, 1173; f, 1223; and g, 1273 K; including insight wide-angle XRD, respectively.

Table 1
Physicochemical properties of the catalysts and their catalytic activities

No	Sample	Surface area ($m^2\ g^{-1}$)	Pore volume ($cm^3\ g^{-1}$)	Pore diameter (Å)	Total acidity (mmol g^{-1})	B/L	BA conversion (%)
1	SBA-15	929	1.36	73.3	–	–	–
2	MCM-41	1155	0.88	30.5	–	–	–
3	MCM-48	1096	0.71	26.1	–	–	–
4	22.4% ZrO_2/SBA-15	426	0.69	71.3	0.30	0.92	27
5	3.36% TPA/SBA-15	341	0.60	70.4	0.29	0.88	21
6	5% TPA/ZrO_2/SBA-15	398	0.63	67.9	0.30	1.01	29
7	15% TPA/ZrO_2/SBA-15	372	0.59	67.7	0.42	1.45	56
8	30% TPA/ZrO_2/SBA-15	329	0.57	67.4	0.35	1.16	43
9	50% TPA/ZrO_2/SBA-15	328	0.53	67.0	0.33	1.12	31
10	70% TPA/ZrO_2/SBA-15	199	0.33	66.7	0.28	0.85	21
11	90% TPA/ZrO_2/SBA-15	199	0.31	66.0	0.26	0.58	15
12	15% TPA/22.4%ZrO_2/MCM-41	516	0.28	19.7	0.33	0.21	44
13	15% TPA/22.4%ZrO_2/MCM-48	540	0.34	17.2	0.25	0.17	10
14	15% TPA/ZrO_2 (Neat)	11	–	–	0.02	1.09	5
	Effect of calcination temperature (K) on 15 wt% TPA/22.4 wt% ZrO_2/SBA-15						
15	923	481	0.63	68.4	0.26	0.58	15
16	1023	410	0.61	68.1	0.33	1.12	32
17	1123	372	0.59	67.7	0.42	1.45	56
18	1173	326	0.47	67.3	0.34	1.19	38
19	1223	249	0.42	66.8	0.26	0.69	29
20	1273	212	0.33	66.1	0.24	0.42	13

All catalysts were calcined at 1123 K except entries 1, 2 and 3. Entries from 6–11 were with 22.4% ZrO_2.
Entry 1, crystal size (by TEM) = 7.1 nm; entry 4, ZrO_2 phase (tetragonal), crystal size (by TEM) = 5.5–6.5 nm and (by XRD) = 6.1 nm; entry 7, ZrO_2 phase (tetragonal), crystal size (by TEM) = 3–4 nm and (by XRD) = 3.4 nm.
Reaction conditions: phenol, 2.52 g (0.026 mol); $PhCH_2OH$, 0.48 g (0.0044 mol); catalyst, 0.15 g; temperature 363 K; time, 3 h.

over SBA-15, it showed corresponding transition of phases only after 923 K.

The textural properties of plain and modified SBA-15 with different loadings of TPA (wt%)/22.4 wt% ZrO_2 are presented in Table 1. It is seen that the surface area, pore size, and pore volume of modified SBA-15 decreased compared with parent SBA-15. This indicates that TPA/ZrO_2 was well dispersed inside the pores of mesoporous channels. The adsorption isotherms and BJH pore size distributions of 15 wt% TPA/22.4 wt% ZrO_2/SBA-15 and parent SBA-15 are shown in Fig. 2. This figure shows that the mesostructure was retained after loading of 15 wt% TPA/22.4 wt% ZrO_2 into SBA-15 and even after calcination up to 1123 K. However, the surface area of the samples up to 50 wt% TPA loading were still $>300\ m^2\ g^{-1}$, and pore volume was in the range of 0.53–0.63 $cm^3\ g^{-1}$ (Table 1), which are sufficient for catalytic func-

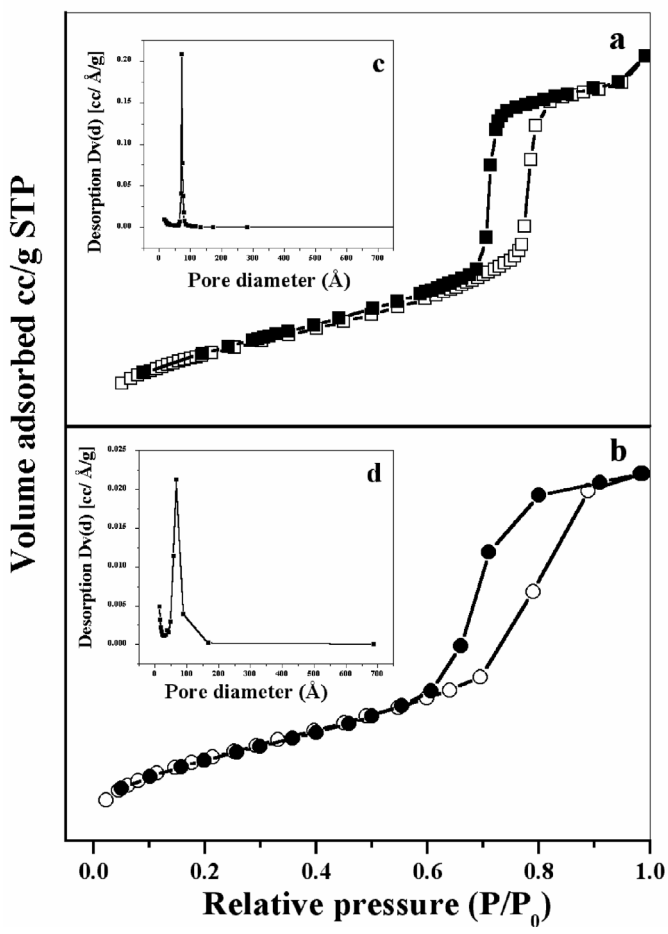

Fig. 2. Nitrogen adsorption isotherms with insight figure of (pore size distribution) of (a) calcined SBA-15 (c) and (b) 15 wt% TPA/22.4 wt% ZrO_2/SBA-15 (d) calcined at 1123 K.

tions. Although the surface areas of modified MCM-41 and MCM-48 were greater than those of corresponding modified SBA-15 samples, their catalytic activities were lower compared with those of 15 wt% TPA/22.4 wt% ZrO_2/SBA-15 (Table 1); this is attributed to blocking of the mesoporous channels of MCM-41 and MCM-48 due to narrow pore diameters. Also, as shown in Table 2, the surface area and pore size of 15 wt% TPA/22.4 wt% ZrO_2/SBA-15 decreased with increasing calcination temperature. The neat 15 wt% TPA/ZrO_2 calcined at 1123 K had low surface area due to sintering of zirconia support, resulting in the formation of larger particles.

The morphology of the supported and unsupported SBA-15 catalyst is shown in Fig. 3. The micromorphology of the supported catalyst remained the same, which was wheat-like even after modification of SBA-15 [29]. TEM measurements were carried out to study the morphology of the parent SBA-15 and TPA/22.4 wt% ZrO_2 modified SBA-15 samples. TEM images of 15 wt% TPA/22.4 wt% ZrO_2/SBA-15 show the retention of the periodic structure of SBA-15 precursor even after calcining at 1123 K. TEM images of 15 wt% TPA/22.4 wt% ZrO_2/SBA-15 (Figs. 4a–d) confirm that the hexagonally arranged mesopores of SBA-15 are retained and TPA/ZrO_2 mainly dispersed inside the pores. Fig. 4a clearly shows the uniform dispersion

Table 2
Study of effects of reaction temperature on conversion of BA and product selectivity

	BA conversion (%)	First-order rate constant	Product selectivity[a] (%)	
			mono-BP	PBE
Temperature				
343	25	0.09	75	22
353	34	0.14	75	22
363	56	0.27	77	20
373	67	0.37	78	19
383	73	0.44	80	17
Regeneration of catalyst				
Fresh	56	–	77	20
First	56	–	77	20
Second	55	–	77	20

Reaction conditions: phenol, 2.52 g (0.026 mol); $PhCH_2OH$ (BA), 0.48 g (0.0044 mol); catalyst, 0.15 g; temperature 363 K; time, 3 h. BP, benzyl phenol; PBE, phenyl benzyl ether; DBE, dibenzyl ether.
[a] DBE, 3% in all the cases.

of TPA/ZrO_2 inside the SBA-15 channels. Figs. 4b and d show the periodic structure of SBA-15 precursor in different beam directions with pore size of 7.1 nm. After supporting SBA-15 with 15 wt% TPA/22.4 wt% ZrO_2, small particles of TPA/ZrO_2 formed inside nanochannels of SBA-15 (Figs. 4c and e). The 22.4 wt% ZrO_2 (5.5–6.5 nm), an optimum loading, was inserted into SBA-15 by the wet impregnation method, which has a higher capacity for monolayer coverage of TPA. The crystallite size of the material calculated from TEM shows that for moderate loading (15 wt%) of TPA, nanosized (3–4 nm) material was formed after wet impregnation over 22.4 wt% ZrO_2/SBA-15 calcined at 1123 K.

The ^{31}P CP-MAS NMR spectra of the supported TPA/ZrO_2 over SBA-15 with different %TPA loadings (i.e., 5, 15, 30, and 50 wt% TPA) are shown in Fig. 5a, and that of 70 and 90 wt% TPA/22.4 wt% ZrO_2/SBA-15 with 3.36 wt% TPA/SBA-15 and 15 wt% TPA/ZrO_2, all calcined at 1123 K, are shown in Fig. 5b. According to previous reports, in bulk TPA, ^{31}P NMR spectra exhibit an intense and sharp line at $\delta = -12$ ppm, showing intact Keggin units [40]. At TPA loading up to 30 wt%, a peak around -12 to -13 ppm was observed. Further increases in loading above 50 wt% produced a small extra peak at -24 ppm, which may be due to partially decomposed TPA with shifts in the original peak. Further increases in loading above 70 wt% produced an extra peak around -30 ppm, attributed to the presence of phosphorous in the decomposition product [10]. In 3.36 wt% TPA/SBA-15, a small peak around -13 ppm was seen, whereas there was complete decomposition of Keggin structures (peak at -30 ppm) in neat 15 wt% TPA/ZrO_2 calcined at 1123 K. An inspection of the chemical shifts (δ) shows their dependence on the loading (%), type of support, and temperature treatment. The TPA derivative species that may give rise to such chemical shifts could be due to partially fragmented Keggin units and also to the strong interaction of TPA with surface ≡Zr–OH groups. The broad line at -12 ppm is probably related to species formed by linking the Keggin units to the zirconia support. Indeed, the first part of the interaction between TPA and zirconia is a protonation of surface hydroxyl groups of zirconia, leading

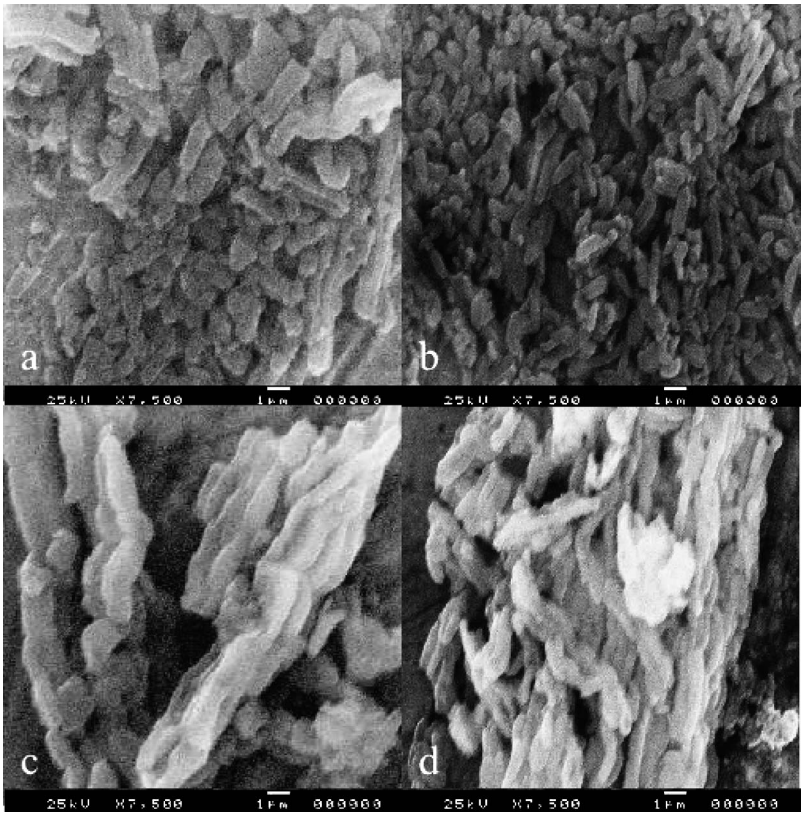

Fig. 3. Scanning electron micrograph of (a) calcined SBA-15 at 813 K, and (b) SBA-15, (c) 22.4 wt% ZrO_2/SBA-15, (d) 15 wt% TPA/22.4 wt% ZrO_2/SBA-15 calcined at 1123 K.

to $(\equiv Zr{-}OH_2)_n{}^+[H_{3-n}W_{12}PO_{40}]^{n-3}$ species [10]. After heating, water is removed, leading to a direct linkage between the polyanion (which has probably retained a structure like that of the Keggin ion) and the support. Because our system deals with high temperatures (1123 K), extensive dehydroxylation of TPA is possible to yield the aforementioned species. When the polyanion decomposes, a new signal appears at −30 ppm. Because the support is heterogeneous, a distribution of surface species will be obtained. Because TPA/ZrO_2 dispersed uniformly in the SBA-15 channels, instead of producing sharp peaks like bulk TPA, line broadening was observed in our system. After modification of SBA-15 with 15 wt% TPA/22.4 wt% ZrO_2, ^{29}Si MAS NMR showed two peaks, at −110 ppm and −112 ppm, corresponding to Q^4, which could be due to the consumption of some silanols during the modification process as has been reported previously [41,42].

The UV–vis spectra of heteropoly acid showed a band at 265 nm for TPA and 275 nm for $ZrOCl_2 \cdot 8H_2O$, in accordance with previous reports [43,44]. TPA-modified samples (i.e., 15 wt% TPA/22.4 wt% ZrO_2/MS) showed characteristic TPA bands at 263–265 nm (Fig. 6) in all of the spectra, which can be assigned to the oxygen–metal charge-transfer band of the tungstophosphate anion $[PW_{12}O_{40}]^{3-}$. However, the 22.4 wt% ZrO_2/SBA-15 showed a band at 275.67 nm, which falls in the nanoparticle region of zirconia as reported previously [44,45]. TPA-modified samples showed only one band, because the ZrO_2 band was overlapped with strong band of TPA (Fig. 6).

Pure silica exhibited IR bands at 1100 and 806 cm^{-1} and a weak shoulder band at 974 cm^{-1} related to surface OH groups. Pure TPA showed characteristic peaks at 1079 cm^{-1} (P–O), 983 cm^{-1} (W=O_t), 893 cm^{-1} (W–O_c–W), and 810 cm^{-1} (W–O_e–W) [46], as shown in Figs. 7a and b. The spectra of ZrO_2 exhibited a wide band at 400–700 cm^{-1} extending up to 1150 cm^{-1} [43]. The spectra of different (%) loading of TPA over ZrO_2/SBA-15 are presented in Fig. 7a. For the TPA/ZrO_2/SBA-15 samples, two bands of TPA appeared at around 983 and 888 cm^{-1}, with the bands around 1079 and 810 cm^{-1} overlapping with the strong bands of SiO_2. The sample with the highest TPA loading (90 wt%) showed characteristic peaks of TPA but excluding a peak at 983 cm^{-1} (W=O_t) due to decomposition of TPA into WO_3 crystallites. Low TPA loading samples showed bands with lower intensity than bulk TPA spectra, due to masking of bands by wide bands of support.

Temperature-programmed desorption of ammonia (NH_3-TPD) was performed to determine the amount and the total acidity in the catalysts. TPD profiles of the catalysts with different (%) TPA loadings in TPA/ZrO_2/SBA-15 calcined at 1123 K are shown in Fig. 8a, and the NH_3-TPD profiles of TPA/ZrO_2 supported on various silica supports, unsupported TPA/ZrO_2, 22.4 wt% ZrO_2/SBA-15, and TPA supported on SBA-15, all calcined at 1123 K, are shown in Fig. 8b. The total acidities of 15 wt% TPA/22.4 wt% ZrO_2/SBA-15 calcined at different temperatures are given in Table 2. Results from Fig. 8a suggest that at TPA loading up to 50 wt%, the samples showed a broad desorption band centered around 523 K, implying medium acidity.

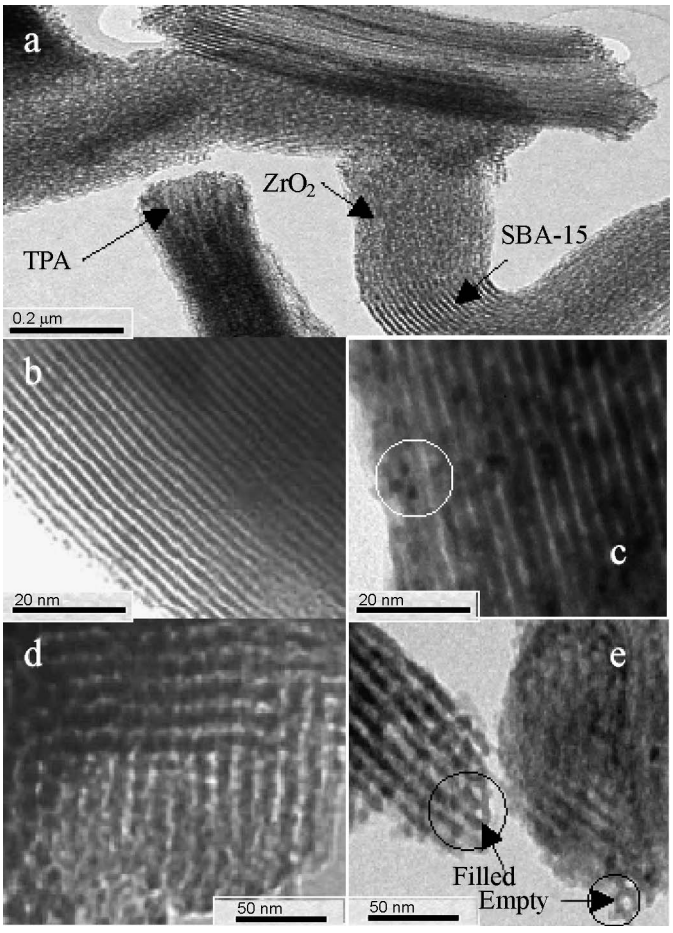

Fig. 4. TEM images of (a) 15 wt% TPA/22.4 wt% ZrO_2/SBA-15 calcined at 1123 K, with the beam perpendicular to the pore direction of (b) SBA-15, (c) 15 wt% TPA/22.4 wt% ZrO_2/SBA-15 and with the beam parallel to the pore direction of (d) SBA-15, (e) 15 wt% TPA/22.4 wt% ZrO_2/SBA-15 calcined at 1123 K.

Further increases in TPA loading (Fig. 8a) produced decreased acidity, which incidentally have lower surface areas. These results indicate that TPA/ZrO_2 dispersed uniformly over SBA-15. According to area under the peak, the supported TPA/ZrO_2 samples showed more acid sites than unsupported TPA/ZrO_2 or 3.36 wt% TPA/SBA-15. Loading of TPA over 22.4 wt% ZrO_2/SBA-15 (Fig. 8b) produced increased acidity and thereby increased catalytic activity in benzylation reaction (Table 1). All samples showed a broad TPD profile, indicating that the surface acid strength was widely distributed. Data on the acidity of different catalyst samples are presented in Table 1. From these data, it is evident that an initial increase in total acidity up to 15 wt% TPA loading is followed by a decrease in total acidity with further increases in TPA loading. It can be concluded that for low TPA loading, the Keggin unit of heteropoly acid retains its structure and acidity, but for higher loading (i.e., above 15 wt% TPA), it decomposes at least partially into its oxides. The highest acidity corresponds to monolayer coverage of TPA (i.e., 15 wt% TPA/22.4 wt% ZrO_2/SBA-15 calcined at 1123 K), where the Keggin structure is intact, as supported by ^{31}P CP-MAS NMR and XRD. Table 2 indicates that the total acidity increases up to 1123 K but that further increases in calcination temperature lead to decreased acidity and also decreased catalytic activity, which is due to decomposition of TPA into WO_3 crystallites.

Brönsted and Lewis acidity of the catalysts were distinguished by pyridine adsorption in situ FTIR spectroscopy. FTIR spectra of pyridine adsorbed on all of the catalysts were recorded from 100–400 °C under a flow of N_2. At 100 °C, important pyridine ring modes occurred at approximately 1609, 1575, 1489, and 1442 cm^{-1} [47,48]. In addition to these vibrations, spectra showed two more peaks, around 1640 and at 1539 cm^{-1}. Pyridine molecules bonded to Lewis acid site absorbed at 1609 and 1442 cm^{-1}, whereas those responsible for Brönsted acid sites (pyridinium ion) showed absorbance

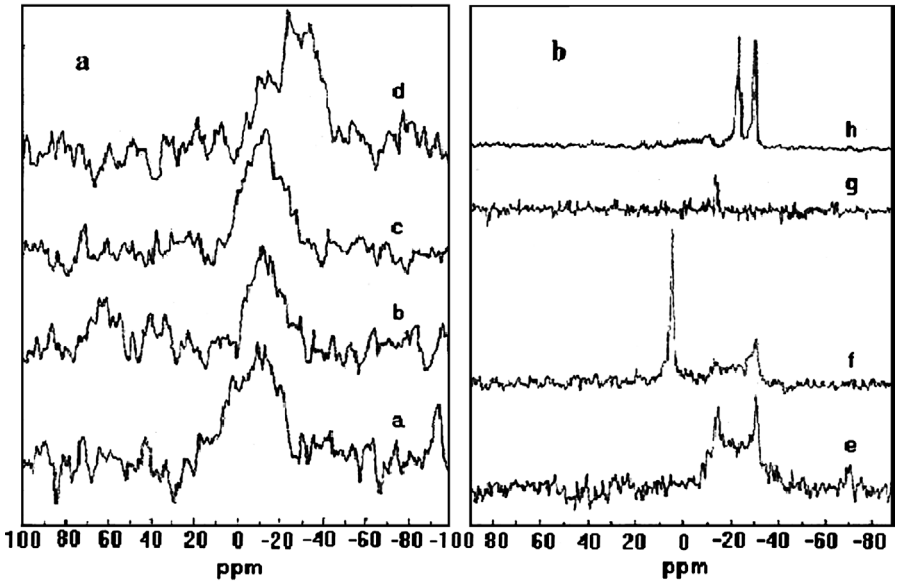

Fig. 5. ^{31}P CP-MAS NMR spectra of TPA/22.4 wt% ZrO_2/SBA-15 with: a, 5; b, 15; c, 30; d, 50; e, 70; f, 90 wt% TPA loading with: g, 3.36 wt% TPA/SBA-15 and h, 15 wt% TPA/ZrO_2 calcined at 1123 K.

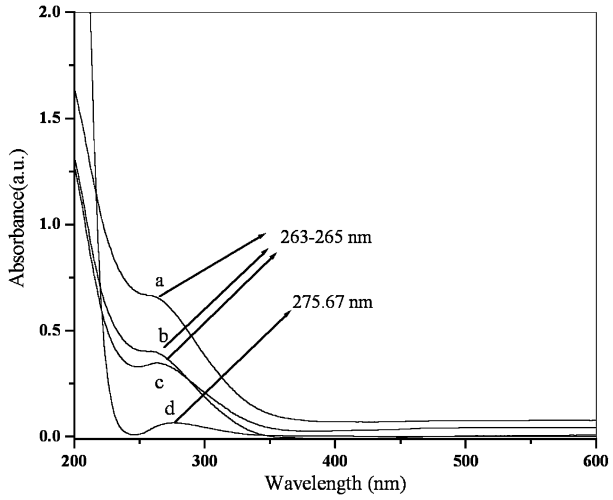

Fig. 6. UV–vis spectra of (a) 15 wt% TPA/22.4 wt% ZrO_2/SBA-15, (b) 15 wt% TPA/22.4 wt% ZrO_2/MCM-41, (c) 15 wt% TPA/22.4 wt% ZrO_2/MCM-48, and (d) 22.4 wt% ZrO_2/SBA-15 calcined at 1123 K.

at 1539 and 1640 cm^{-1}. The Brönsted/Lewis (B/L) site ratio was calculated from the IR absorbance intensities [49] of bands at 1539 (B) and 1442 (L) cm^{-1} for different catalysts along with different (%) loadings of TPA, and were compared with catalytic activity in phenol benzylation with different calcination temperatures for 15 wt% TPA/22.4 wt% ZrO_2/SBA-15; the results are given in Table 1. It was found that the B/L ratio increased with increased TPA loading up to 15 wt%, but then decreased with further increases in TPA loading. Thus the sample with 15 wt% TPA/22.4 wt% ZrO_2/SBA-15 had the highest acidity, due to the monolayer coverage of TPA on ZrO_2 finely dispersed in SBA-15 channels. But on further increases in TPA loading, the B/L ratio decreased, and hence the catalytic activity also decreased. The decrease in B/L ratio and activity was due to decomposition of TPA, which exceeded monolayer coverage at higher TPA loadings. Brönsted acidity of 15 wt% TPA/22.4 wt% ZrO_2/SBA-15 calcined at 1123 K (Table 1), which could be explained as, during calcination dehydroxylation of support occurs, resulting in crystallization. In this process, the interaction of TPA and support is partially weakened, giving rise to free H^+ ions, which act as Brönsted

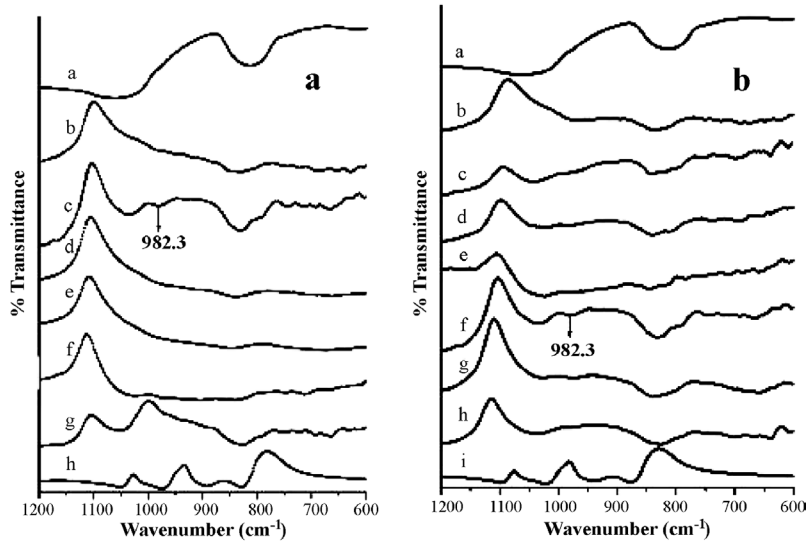

Fig. 7. (a) FTIR spectra: a, pure silica, TPA/22.4 wt% ZrO_2/SBA-15 with: b, 5; c, 15; d, 30; e, 50; f, 70; g, 90 wt% TPA loading calcined at 1123 K; and, h pure TPA. (b) FTIR spectra: a, pure silica, 15 wt% TPA/22.4 wt% ZrO_2/SBA-15 calcined at b, 773; c, 923; d, 1023; e, 1123; f, 1173; g, 1223; h, 1273 K; and, i pure TPA.

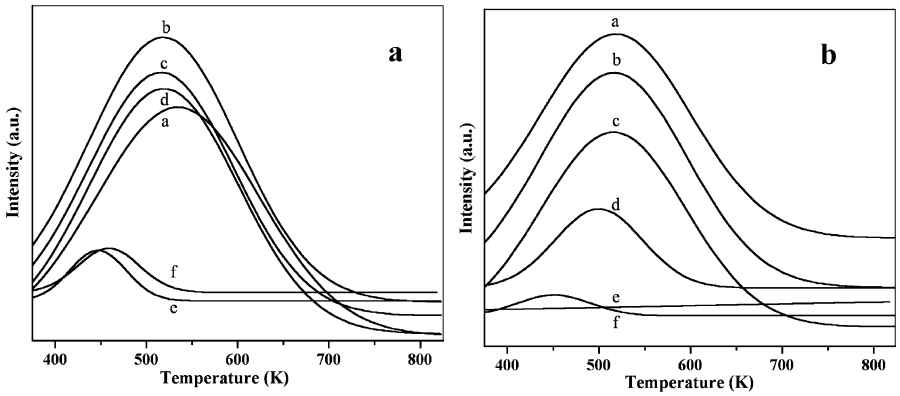

Fig. 8. (a) NH_3-TPD profiles: TPA/22.4 wt% ZrO_2/SBA-15 with a, 5; b, 15; c, 30; d, 50; e, 70; f, 90 wt% TPA loading and (b) 15 wt% TPA/22.4 wt% ZrO_2 supported over a, SBA-15; b, MCM-41; c, MCM-48; d, 22.4 wt% ZrO_2/SBA-15; e, 3.36 wt% TPA/SBA-15; f, neat 15 wt% TPA/ZrO_2 calcined at 1123 K.

acid sites. Brönsted acidity increased with increasing calcination temperature up to 1123 K (i.e., at monolayer coverage) and B/L ratio decreased with further increases in calcination temperature.

TG-DTG spectra of all the samples dried at 100 °C are shown in Fig. 9. Under similar measurement conditions, TG-DTG analysis of pure TPA hydrate showed three stages of weight loss (endothermic effect) [50]. The first weight loss, around 3–6%, occurred from room temperature to 125 °C, due to the loss of physisorbed water. The second one, from 130–305 °C, accounted for the loss of crystallization water, and the third, in the range of 370–550 °C, was due to the loss of 1.5 H_2O molecules originating from all acidic protons. The total weight loss of the sample corresponded to 21 H_2O per Keggin unit. Furthermore, it showed a break at 350 °C, due to the decomposition of heteropoly acid [51]. The TGA behavior was similar in all of the TPA/ZrO_2-supported samples, showing the first weight loss of about 3% in all TPA/ZrO_2 supported over SBA-15 samples, corresponding to physisorbed water. But the MCM-41 and MCM-48 supports showed heavy weight loss, corresponding to physisorbed water, compared with the SBA-15-supported samples. But none of the supported samples showed an appreciable change in weight loss until 900 °C, indicating increasing stability of TPA. The neat 15 wt% TPA/ZrO_2 sample exhibited weight loss corresponding to physisorbed water along with another weight loss around 450–600 °C that may be due to a phase transition from tetragonal to monoclinic.

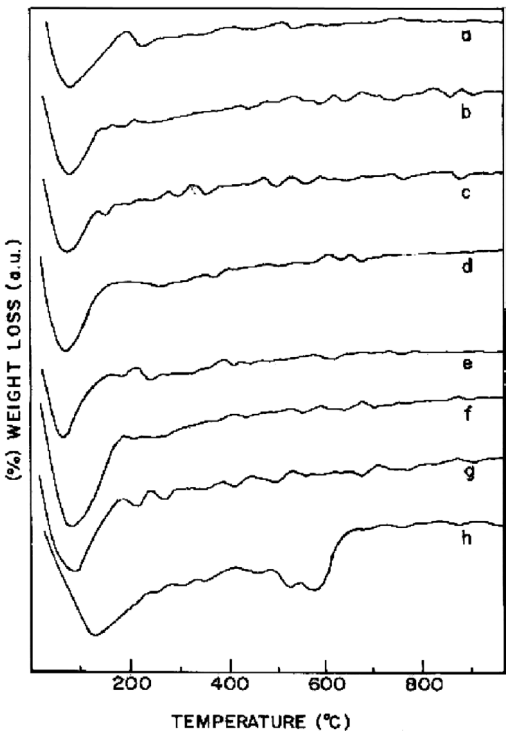

Fig. 9. TG-DTG curves of (a) 22.4 wt% ZrO_2/SBA-15, TPA/22.4 wt% ZrO_2/SBA-15 with (b) 5, (c) 15, (d) 30, (e) 50 wt% TPA loading with (f) 15 wt% TPA/22.4 wt% ZrO_2/MCM-41, (g) 15 wt% TPA/22.4 wt% ZrO_2/MCM-48, and (h) 15 wt% TPA/ZrO_2 calcined at 1123 K.

3.2. Catalytic activity

The liquid phase benzylation of phenol with BA was carried out using TPA/ZrO_2 formed in SBA-15 channels as a catalyst; the reaction followed as shown in the first scheme (Fig. 11). Data on the catalytic performance of various (%) TPA-loaded catalysts calcined at 1123 K, along with reaction conditions and data on the catalytic activity of 15 wt% TPA/22.4 wt% ZrO_2/SBA-15 calcined at different temperatures are presented in Table 1. Benzylation of phenol with 15 wt% TPA/22.4 wt% ZrO_2/SBA-15 calcined at 1123 K catalysts under selected reaction conditions (363 K, 3 h, 150 mg catalyst, phenol/BA molar ratio of 6) gave 77% *ortho*- and *para*-BP (A) plus (B) (i.e., mono-BP as the main product), 20% benzyl phenyl ether (C), and 3% benzyl ether (D).

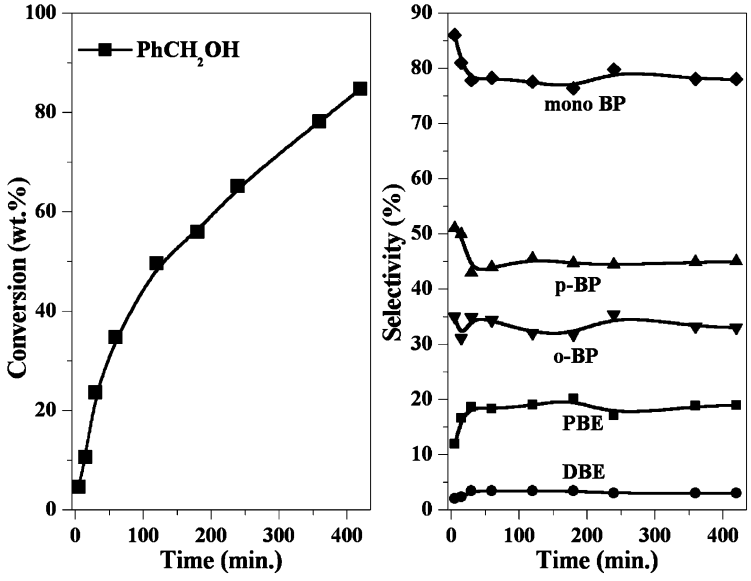

Fig. 10. Effect of time on stream on BA conversion and product selectivity. Conditions: phenol, 2.52 g (0.026 mol); BA, 0.48 g (0.0044 mol); catalyst weight, 150 mg; phenol/BA (mol ratio), 6:1; temperature, 363 K; time, 3 h. BP, benzyl phenol; PBE, phenyl benzyl ether; DBE, dibenzyl ether.

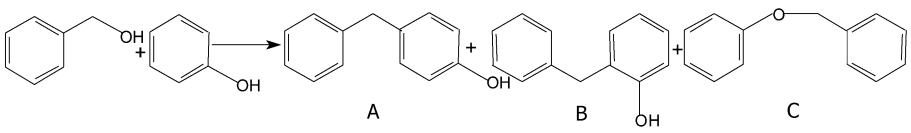

Scheme 1.

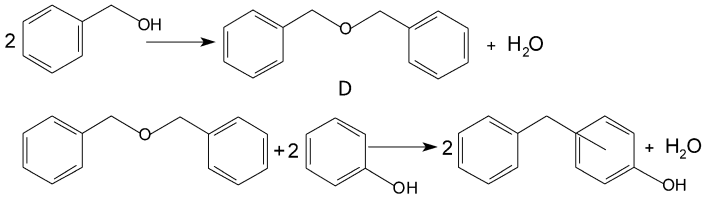

Scheme 2.

Fig. 11.

The 15 wt% TPA/22.4 wt% ZrO_2/SBA-15 calcined at 1123 K gave the highest conversion of BA (56%) under selected reaction conditions (Table 1). The effect of TPA loading and calcination temperature on BA conversion obtained is shown in Table 1. Combining these findings with the results of FTIR pyridine adsorption data reveal that the B/L ratio of the catalysts increased up to 15% TPA loading and that 15 wt% TPA/22.4 wt% ZrO_2/SBA-15 calcined at 1123 K had the highest B/L ratio and gave the highest catalytic activity in benzylation of phenol under reaction conditions. In this catalytic system, zirconia alone loaded on mesoporous silica support (i.e., 22.4 wt% ZrO_2/SBA-15 calcined at 1123 K) showed some catalytic activity, whereas zirconia loaded on 15 wt% TPA showed a two-fold increase in catalytic activity (Table 1). This illustrates the role of the composite materials and the effect of zirconia on the acidity function of TPA, which enhance catalytic activity. Accordingly, ZrO_2 is considered a weakly acidic oxide composed of mainly Lewis-type acid sites [52]. In contrast, solid H_3 $[PW_{12}O_{40}]\cdot 6H_2O$ contains acid sites stronger than $H_0 = -8.2$ [53]. Nevertheless, it has been reported that pure TPA is characterized by mainly Brönsted-type acidity [54]. On calcination, TPA impregnated on a freshly precipitated ZrO_2 underwent dehydroxylation and concomitant structure transformation, implying that some (OH) groups may react with TPA protons. Assuming that some TPA protons will react with (OH) groups in hydrated zirconia, it would be reasonable to expect that some terminal W=O bonds of TPA might react with partially dehydroxylated $(Zr(–O)_3)^+$ species to form anchored TPA species (e.g., the formation of Zr–O–W bonds). These TPA species would exert an electron-withdrawing effect on surface Zr^{4+} cations, making them to behave as strong Lewis acid sites. But these phenomena occurred at temperatures up to 673 K. Accordingly, the strongly acidic properties of TPA/ZrO_2 could be attributed to electron-withdrawing effects similar to those ascribed to Zr-bonded sulfate groups [55–57]. Above 673 K, all dehydrated zirconia reacted with TPA. In this catalytic system, the fact that TPA remained amorphous at temperatures up to 923 K suggests strong interactions between heteropoly acid and zirconia at the structural level. But crystallite size measurements (Table 1) showed that TPA content inhibited crystal growth of the catalyst material; this behavior is very common in mixed materials containing a crystalline and an amorphous phase together. The crystalline material is usually surrounded by an amorphous phase layer, which acts as a physical barrier to hinder the sintering process and inhibit crystallite growth [58,59]. Keeping in mind all of these findings, we hypothesize that at calcination above 923 K, the interaction between TPA and zirconia may weaken to monolayer coverage (15 wt% and 1123 K), making TPA protons free for reactions to proceed and thereby increasing Brönsted acidity and total acidity (from the increase in Lewis acidity due to zirconia). With further increases in calcination temperature above 1123 K, possibly due to multilayer formation, bulk properties of TPA will be more predominant, causing destruction of TPA to yield WO_3 crystallites, as was partially proved by NMR. Besides sulfate ions, tungstate and molybdate oxoanions also produce strong acidic sites when deposited on hydroxylated zirconia [60]. The interaction between the TPA and zirconia is responsible for the high acidity.

The 15 wt% TPA/22.4 wt% ZrO_2 modified SBA-15 catalyst showed higher catalytic activity than the 15 wt% TPA/22.4 wt%ZrO_2 modified MCM-41 and MCM-48 catalysts calcined at 1123 K. We hypothesize that large TPA clusters (∼12 Å) can readily clog the pores during solution impregnation when support pore sizes are smaller, as in the case of MCM-41 (30.5 Å) and MCM-48 (26.1 Å). But when the zirconia along with TPA was dispersed in the mesoporous channels of supports at high temperature calcination, the acidity of the catalysts was altered, becoming higher with SBA-15. In contrast, TPA/ZrO_2 is likely have a better chance to uniformly coat the pores when the support pore size is sufficiently large, as in the case of SBA-15 (73.3 Å) compared with MCM-41 and MCM-48. However, the neat 15 wt% TPA/ZrO_2 calcined at 1123 K showed poor catalytic activity with conversion of BA (5%), at least 10 times less than that of the modified 15 wt% TPA/22.4 wt% ZrO_2/SBA-15 calcined at 1123 K under the same reaction conditions. This enhanced activity could be due to more accessible protons when 15 wt% TPA/ZrO_2 is supported on large surface area and the larger pore diameters of

the SBA-15 mesoporous silica material. Hence this catalyst was used in catalytic studies to assess activity in the test reaction.

The effect of temperature on conversion and product selectivity was studied in the range 343–383 K; the results are presented in Table 2. With increasing temperature, BA conversion increased up to 73%, whereas selectivity for mono-BP increased and that of PBE decreased. Benzylation of phenol by BA was carried out with catalyst, 0.150 g (3 wt% of total reaction mixture), phenol/BA molar ratio 6 at 363 K for 7 h to investigate the effect of BA conversion and product selectivity as functions of time (Fig. 10). With increasing time, BA conversion increased to a maximum of 85% after 7 h with 78% selectivity for mono-BP, 19% for phenyl benzyl ether (PBE), and the remainder for DBE.

To reuse the catalyst, the catalyst used in the first cycle of the reaction was separated by filteration, washed three times with 1,2-dichloromethane, dried in an oven at 100 °C for 24 h, and activated at 500 °C for 4 h in an air. The activated catalyst was used for benzylation of phenol with BA under selected reaction conditions. This same procedure was repeated for the second cycle; the data on the conversion of BA are presented in Table 2. From these results, we can conclude that there was no appreciable loss in catalytic activity and product selectivity in the two cycles, and that the catalyst can be reused.

To check the leaching of TPA into the reaction mixture, the reaction was carried out for 2 h under selected reaction conditions using fresh 15 wt% TPA/22.4 wt% ZrO_2/SBA-15 calcined at 1123 K. The reaction was stopped, the catalyst was separated by filteration, and then the filtrate was stirred for 1 h under the same reaction conditions. It was found that in the absence of the catalyst, there was no further increase in the conversion of BA, indicating the lack of TPA leaching into the reaction mixture. This observation confirmed that the reaction was catalyzed heterogeneously. In addition, leaching of TPA (i.e., dissolution of P or W) into the hot filtrate was tested by inductively coupled plasma-optical emission spectroscopy (ICP-OES), which found the complete absence of P or W.

Two reaction schemes have been proposed for phenol benzylation with BA (Fig. 11) [61]. The first scheme involves the direct formation of BP by alkylation of phenol with BA, whereas the second scheme involves a two-step process in which PBE is formed and then subsequently converted to BP. BA gave PBE as the product in a parallel reaction. With increasing temperature, PBE decreased, possibly due to internal transformation of O– and C–, an alkylated product. BP is a primary product, and PBE is a primary and/or secondary product that transforms during reaction to BP; such rearrangement occurs on heating or contact with an acid catalyst.

Because benzylation of phenol by BA involves two consecutive steps to form BP (Fig. 11), the standard equations for a first-order series reaction, $C_A/C_{A_0} = e^{-k_1 t}$, were used to determine the rate constant, where C_A and C_{A_0} are the concentration of BA at initial time and at time t, respectively. The rate constants calculated at different temperatures are presented in Table 2. It is seen that k_1 increased with increasing temperature. The activation energy for benzylation of phenol was calculated from the Arrhenius graph and was found to be 10.38 kcal/mol.

4. Conclusions

The results presented in this work demonstrate that TPA/ZrO_2 dispersed uniformly inside the mesopores of SBA-15 formed nanocomposite material at a calcination temperature of 1123 K. The formation of nanosized (3–4 nm) TPA/ZrO_2 was found to depend on (%) TPA loading, monolayer coverage on ZrO_2, geometry, the nature of mesoporous supports, and calcination temperature. Among mesoporous silica supports, SBA-15 was better and provided higher thermal stability and catalytic activity than MCM-41 and MCM-48 in benzylation reactions. The mesoporous material has an advantage in the formation of nanosized and catalytically active TPA/ZrO_2 by stabilizing zirconia in tetragonal phase at 1123 K, which provided higher catalytic activity than the neat TPA/ZrO_2 in benzylation reactions. The higher stability and catalytic activity can be achieved by incorporating heteropoly acid (TPA)/ZrO_2 in supports like SBA-15 to get greater catalytic activity (ten-fold higher) than with the corresponding neat TPA/ZrO_2 catalyst.

Acknowledgments

The authors thank DST-SERC, New Delhi for financial support. Sawant also acknowledges the support of a Senior Research Fellowship from CSIR, New Delhi.

References

[1] A. Corma, A. Martinez, Catal. Rev. Sci. Eng. 35 (4) (1993) 483.
[2] F.W. Kirsch, J.D. Potts, D.S. Barmby, J. Catal. 27 (1972) 142.
[3] J. Weitkamp, Stud. Surf. Sci. Catal. 5 (1980) 65.
[4] A. Corma, A. Martinez, C. Martinez, J. Catal. 146 (1994) 185.
[5] J. Kaur, K. Griffin, B. Harrison, I.V. Kozhevnikhov, J. Catal. 208 (2002) 448.
[6] J.A. Kocal, V.V. Bipin, I. Tamotsu, Appl. Catal. A 221 (2001) 295.
[7] I.V. Kozhevnikov, M.N. Timofeeva, J. Mol. Catal. 75 (1992) 179.
[8] T. Blasco, A. Corma, A. Martinez, P. Martinez-Escolano, J. Catal. 177 (1988) 306.
[9] B.M. Devassy, S.B. Halligudi, S.G. Hegde, A.B. Halgeri, F. Lefebvre, Chem. Commun. 10 (2002) 1074.
[10] E. Lopez-Salinas, J.G. Hernandez-Corez, I. Schifter, E. Torres-Garcia, J. Navarrete, A. Gutierrez-Carillo, T. Lopez, P.P. Lottici, D. Bersani, Appl. Catal. A 193 (2000) 215.
[11] D.P. Sawant, B.M. Devassy, S.B. Halligudi, J. Mol. Catal. 217 (2004) 211.
[12] K. Shimizu, T.N. Venkataraman, W. Song, Appl. Catal. A 225 (2002) 33.
[13] D.G. Barton, S.L. Soled, G.D. Meitzner, G.A. Fuentes, E. Iglesia, J. Catal. 181 (1999) 57.
[14] J.G. Santeisteban, J.C. Vartuli, S. Han, R.D. Bastain, C.D. Chang, J. Catal. 168 (1997) 431.
[15] H. Takahashi, B. Li, T. Sasaki, C. Miyazaki, T. Kajino, S. Inagaki, Chem. Mater. 12 (2000) 3301.
[16] H. Li, R. Wang, Q. Hong, L. Chen, Z. Zhong, Y. Koltypin, J. Calderon-Moreno, A. Gedanken, Langmuir 20 (2004) 8352.
[17] L. Marosi, G. Cox, A. Tenten, H. Hibst, J. Catal. 194 (2000) 140.
[18] T. Okuhara, C. Hu, M. Hashimoto, M. Misono, Bull. Chem. Soc. Jpn. 67 (1994) 1186.
[19] Y. Wu , X. Ye, X. Yang, X. Wang, W. Chu, Y. Hu, Ind. Eng. Chem. Res. 35 (1996) 2546.
[20] I.V. Kozhevnikov, K.R. Kloetstra, A. Sinnema, H.W. Zandbergen, H. van Bekkum, J. Mol. Catal. A Chem. 114 (1996) 287.
[21] A. Ghanbari-Siahkali, A. Philippou, J. Dwyer, M.W. Anderson, Appl. Catal. A 192 (2000) 57.
[22] Z. Zhao, W. Ahn, R. Ryoo, Stud. Surf. Sci. Catal. 146 (2003) 657.

[23] J. Wang, Z. Hai-Ou, Catal. Lett. 93 (2004) 209.
[24] G.D. Yadav, H. Manyar, Microporous Mesoporous Mater. 63 (2003) 85.
[25] R.L. McCormick, S.K. Boonrueng, A.M. Herring, Catal. Today 42 (1998) 145–157.
[26] J.A. Dias, E. Caliman, S.C.L. Dias, M. Paulo, A. Thyrso, C.P. deSouza, Catal. Today 85 (2003) 39–48.
[27] E. Lopez-Salinas, J.G. Hernández-Cortéz, I. Schifter, E. Torres-Garcia, J. Navarrete, A. Gutierrez-Carrillo, T. López, P.P. Lottici, D. Bersanni, Appl. Catal. A 193 (2000) 215–225.
[28] S. Hodjati, K. Vaezzadeh, C. Petit, V. Pitchon, A. Kiennemann, Top. Catal. 16–17 (2001) 151–155.
[29] D. Zhao, J. Feng, Q. Huo, N. Melosh, G.H. Fredrickson, B.F. Chmelka, G.D. Stucky, Science 279 (1998) 548.
[30] X. Wang, M.V. Landau, H. Rotter, L. Vradman, A. Wolfson, A. Erenburg, J. Catal. 222 (2004) 565.
[31] M.V. Landau, L. Titleman, L. Vradman, P. Wilson, Chem. Commun. (2003) 594.
[32] H.-W. Voges, in: B. Elvers, S. Hawkins, G. Schulz (Eds.), Ullmann's Encyclopedia of Industrial Chemistry, vol. 19, VCH, Weimheim, Germany, 1991, p. 328.
[33] B.M. Devassy, G.V. Shanbhag, F. Lefebvre, W. Böhringer, J. Fletcher, S.B. Halligudi, J. Mol. Catal. A: Chem. 230 (2005) 113.
[34] T. Matsuura, Y. Ohkatsu, Polym. Degrad. Stab. 70 (2000) 59.
[35] M. Hartmann, S. Racouchot, C. Bischof, Microporous Mesoporous Mater. 27 (1999) 309.
[36] K. Schumacher, M. Grün, K.K. Unger, Microporous Mesoporous Mater. 27 (1999) 201.
[37] D. Zhao, J. Sun, Q. Li, G.D. Stucky, Chem. Mater. 12 (2000) 275.
[38] J. He, X. Duan, C. Li, Mater. Chem. Phys. 71 (2001) 221.
[39] H.P. Klug, L.E. Alexander, X-Ray Diffraction Procedures, Wiley, New York, 1974.
[40] M. Misono, Chem. Commun. (2001) 1141.
[41] M.W. McKittrick, C.W. Jones, Chem. Mater. 15 (2003) 1132.
[42] A.S. Maria Chong, X.S. Zhao, A.T. Kwtedji, S.Z. Qiao, Microporous Mesoporous Mater. 72 (2004) 33.
[43] L. Pizzio, P. Vázquez, C. Cáceres, M. Blanco, Catal. Lett. 4 (2001) 77.
[44] A.V. Emeline, G.V. Kataeva, A.S. Litke, A.V. Rudakova, V.K. Ryabchuk, N. Serpone, Langmuir 14 (1998) 5011.
[45] J. Joo, T. Yu, Y.W. Kim, H.M. Park, F. Wu, J.Z. Zhang, T. Hyeon, J. Am. Chem. Soc. 125 (2003) 6553.
[46] W. Kuang, A. Rives, M. Fournier, R. Hubaut, Appl. Catal. A 250 (2003) 221.
[47] C.H. Cline, J. Turkevich, J. Chem. Phys. 12 (1944) 300.
[48] C. Morterra, A. Chiorino, E. Ghiottiand, E. Garrone, J. Chem. Soc., Faraday Trans. I 75 (1979) 271.
[49] B.H. Davis, R.A. Keogh, S. Alerasool, D.J. Zalewski, D.E. Day, P.K. Doolin, J. Catal. 183 (1999) 45.
[50] I.V. Kozhevnikov, Catalysis by Polyoxometalates, Catalysts for Fine Chemical Synthesis, vol. 2, Wiley, 2002, p. 15.
[51] T. Okuhara, N. Mizuno, M. Misono, Adv. Catal. 41 (1996) 113.
[52] Y. Nakano, T. Iizuka, H. Hattori, K. Tanabe, J. Catal. 57 (1978) 1.
[53] Y. Saito, P.N. Cook, H. Niiyama, E. Echigoya, J. Catal. 95 (1985) 49.
[54] K. Tanabe, M. Misono, Y. Ono, H. Hattori, Stud. Surf. Sci. Catal. 51 (1989) 169.
[55] T. Jin, T. Yamaguchi, K. Tanabe, J. Phys. Chem. 90 (1986) 4794.
[56] K. Tanabe, H. Hattori, T. Yamaguchi, Crit. Rev. Surf. Chem. 1 (1990) 1.
[57] C.J. Norman, P.A. Goulding, P.J. Moles, Stud. Surf. Sci. Catal. 90 (1994) 269.
[58] D.H. Aguilar, L.C. Torres-Gonzalez, L.M. Torres-Martinez, T. Lopez, P. Quintana, J. Solid State Chem. 158 (2001) 349.
[59] E. Torres-Garcia, G. Rosas, J.A. Ascencio, E. Haro-Poniatowski, R. Perez, Appl. Phys. A 79 (2004) 401.
[60] K. Arata, Adv. Catal. 37 (1990) 165.
[61] A.B. Deshpande, A.R. Bajpai, S.D. Samant, Appl. Catal. A 209 (2001) 229.